https://dx.doi.org/10.1016/j.chemosphere.2022.134816

Impact of NO_x reduction on long-term surface ozone pollution in roadside and suburban Hong Kong: Field measurements and model simulations

Lewei Zeng[1,2], Jin Yang[2], Hai Guo[*,2], Xiaopu Lyu[2]

1 College of Chemistry and Environmental Engineering, Shenzhen University, Shenzhen, China

2 Department of Civil and Environmental Engineering, The Hong Kong Polytechnic University, Hong Kong, China

*Corresponding author: ceguohai@polyu.edu.hk

Abstract

Continuous measurements of ozone (O_3) and nitrogen oxides (NO_x=NO+NO_2) were conducted from 2007 to 2019 in Hong Kong in order to evaluate the effectiveness of control strategies for NO_x emission from diesel commercial vehicles (DCV). DCV control programs were periodically applied in three phases starting from 2007, 2010 and 2014. It was found that NO and NO_2 levels decreased during the study period but more dramatically after the implementation of DCV Phase III than pre-DCV Phase III. Source apportionment analysis confirmed that the ambient NO and NO_2 in Hong Kong attributed to the regulated DCV emissions in Phase III reduced at rates of 5.1-14.4 ppbv/yr in roadside environment and 1.6-3.1 ppbv/yr in suburban area. Despite overall NO_x reduction, increased NO_2/NO_x ratios were recorded during the study period possibly due to the application of diesel particulate filter (DPF) in DCVs. However, after introducing DCV Phase III, observed O_3 values experienced more

dramatic increasing trends in most areas of Hong Kong than pre-DCV Phase III. Model simulations revealed that O_3 production rate kept increasing and turned to be less sensitive to NO_x from 2014 to 2019. On the roadside, net O_3 production rate was more than doubled during 2014-2019 owing to NO_x reduction. Moreover, the levels of oxidants (OH, HO_2 and RO_2) were 1.5-5 times those before 2014. In suburban environment, NO_x reduction also facilitated O_3 production and radical cycling, but made smaller contributions than those on the roadside during 2014-2019. This study unraveled that NO_x reductions benefited from DCV regulations caused increase in surface O_3 and fueled O_3 photochemistry in various environments. More stringent control measures on emissions of VOCs, especially those with high OH reactivity, might help to better mitigate O_3 pollution.

Keywords: *Nitrogen oxides*, *long-term variation*, *source apportionment*, *ozone photochemistry*, *ozone-precursors relationship, diesel commercial vehicles*

1 Introduction

Nitrogen oxides (NO_x), the reactive nitrogen in the atmosphere, adversely affect human health (Hoek et al., 2002; Samoli et al., 2006) and cause eco-environmental problems, such as acid rain and algae blooms (Liu et al., 2020). They are also important precursors for the formation of tropospheric ozone (O_3), which further leads to human health risks and reduced vegetation yields (Bell et al., 2004). As the most common air pollutant, O_3 is generated through photochemical reactions with the participation of volatile organic compounds (VOCs), NO_x and carbon monoxide (CO)

in the presence of sunlight (Atkinson, 2000). In view of the nonlinear relationship between O_3 and precursors, mitigating O_3 pollution has become a complex issue.

In urban area, O_3 production is generally in a VOC-limited regime due to intensive anthropogenic emissions (Lu et al., 2019). Road transport is considered as a significant contributor to ambient NO_x, accounting for more than 40 %, as well as VOCs, according to emission inventories in different countries (EEA, 2015; HKEPD, 2020). In order to alleviate surface O_3 and NO_x pollution, many parts of the world, including Hong Kong, which is a densely populated city in China, have implemented stringent control strategies to reduce vehicular emissions, especially diesel vehicle emissions. The design and installation of exhaust gas recirculation (EGR) and selective catalytic reduction (SCR) devices in diesel vehicles aimed to reduce NO_x emissions can be traced back to the 1970s (Teshirogi et al., 1974). Since then, stricter fuel and emission standards have been adopted, and substandard vehicles have been progressively phased out worldwide (Guan et al., 2014; Jiang et al., 2016; Reşitoğlu et al., 2015; Takekawa et al., 2013; Wu et al., 2012). For example, the Chinese government promoted the Clean Air Action Plan in 2013, in which the control of vehicular emissions is an important component (Zhang et al., 2019; Zhao et al., 2013). In Hong Kong, emission control strategies for diesel commercial vehicles (DCVs) began in April 2007 (HKEPD, 2019a). The first stage ended in March 2010, and pre-Euro and Euro I DCVs were replaced or upgraded. The measures in the second stage (July 2010 – June 2013) emphasized the upgrade of Euro II DCVs while the third stage (March 2014 – December 2019) was implemented to phase out all pre-Euro IV

DCVs. Meanwhile, SCRs and diesel particulate filter (DPF) were applied on Euro II and III franchised buses. Table S1 summarizes all stages of DCVs control measures in Hong Kong. Lyu et al. (2017) evaluated the impact of DCVs control measures in Phases I and II on VOCs and O_3 formation; however, the effectiveness of control measures in DCV Phase III on NO_x reduction and the subsequent impact on O_3 pollution has not been investigated yet.

Owing to strict regulations, NO_x values in urban environments have mainly shown downward trends in the past two decades in Europe (Beevers et al., 2012; Carslaw et al., 2011; Macdonald et al., 2021; Vohra et al., 2021), in North America (Geddes et al., 2009; Simon et al., 2015), and in part of East Asia (Itano et al., 2007; Pandey et al., 2008; Shon et al., 2011; Zhang et al., 2014). However, contrary to the decreasing trends of O_3 in most cases in Europe and North America, long-term observations revealed that O_3 in cities in East Asia, especially in China, increased during this period (Li et al., 2020; Lu et al., 2020). With the aid of chemical transport model simulations, previous studies indicated that, among all possible driving factors, NO_x reduction was the main cause of O_3 increase in China (Liu and Wang, 2020; Wang et al., 2019). However, the underlying chemical mechanisms are missing.

In this study, O_3 and NO_x were continuously monitored from 2007 to 2019 over the whole territory of Hong Kong. Temporal variations of O_3 and NO_x were investigated and the effectiveness of the DCV Phase III on NO_x variations was evaluated based on measurement data and source apportionment analysis. Moreover, by adopting a photochemical box model coupling with near-explicit master chemical mechanism

(PBM-MCM), we for the first time elucidated the impact of NO_x variations on O_3 formation and attempted to provide a scientific basis for mitigating O_3 pollution in Hong Kong.

2 Data and methods

2.1 Data source

The Hong Kong government set up a complete monitoring network in the 1990s, measuring ambient trace gases, including O_3, nitric oxide (NO), nitrogen dioxide (NO_2), CO and sulfur dioxide (SO_2). Considering the percentage of valid data, we selected two roadside sites, eleven general ambient sites spreading in urban/suburban areas, and one rural site in this study. We acquired hourly monitoring data of the above five air pollutants during April 2007 – March 2019 from the website of Hong Kong Environmental Protection Department (HKEPD, https://cd.epic.epd.gov.hk/EPICDI/air/station/). Geographical locations of the selected 14 monitoring stations are shown in Figure 1, including two roadside sites, 11 general urban/suburban sites and one general rural site. Table S2 describes each monitoring station in detail, including the invalid data period.

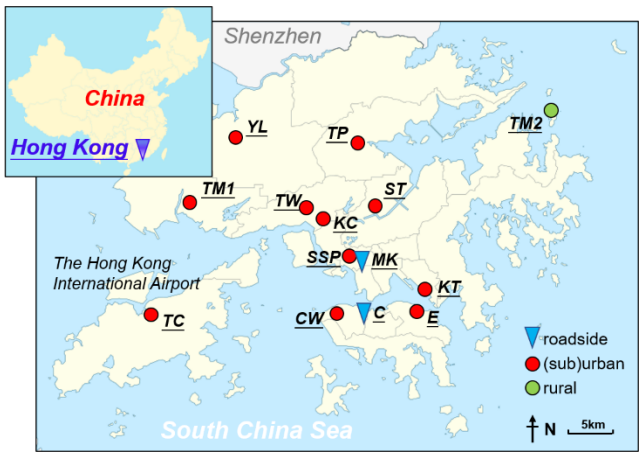

Figure 1. Geographical locations of monitoring stations in Hong Kong. Full names

and abbreviations of monitoring stations are listed in Table S2.

In addition, real-time VOCs were continuously measured at one roadside site (MK) and one suburban site (TC) from 2013 to March 2019. Totally 27 C_2-C_9 hydrocarbons, including 10 alkanes, 9 alkenes/alkynes and 8 aromatics, were identified and quantified by an online gas chromatography system (Syntech Spectra GC 955, Series 600/800) with a resolution of 30 min. Data were acquired and averaged into hourly values for analysis. Analytical instruments and quality control procedures were presented in previous studies (HKEPD, 2019b; Lyu et al., 2016).

2.2 Simulation of in-situ photochemistry

In this study, we applied a PBM-MCM model developed by our own group to simulate the in-situ photochemistry at TC and MK sites in Hong Kong. Mixing ratios of trace gases (*i.e.,* NO, NO_2, CO, SO_2 and O_3) and VOCs from 7 am to 7 pm were input into this observation-based model to reproduce the real atmospheric conditions in the study area. Meteorological parameters, such as atmospheric pressure, temperature and relative humidity, were acquired from the Hong Kong Observatory and constrained in the model during the simulations. The developed PBM-MCM model has been widely utilized in Hong Kong and the model performance has been repeatedly testified in previous studies (Lyu et al., 2016, 2017; Wang et al., 2017; Zeng et al., 2018).

Index of agreement (IOA) represents the agreement between observed values (O_i) and simulated values (S_i), as described in Equation 1. $\bar{O}$ stands for the mean of observed data over n samples. Higher IOA value ($0 < \mathrm{IOA} < 1$) indicates better model

performance.

$$IOA = 1 - \frac{\sum_{i=1}^{n}(O_i - S_i)^2}{\sum_{i=1}^{n}(|O_i - \bar{O}| + |S_i - \bar{O}|)^2} \quad (1)$$

Since regional transport is not fully considered in the model, there might be differences between the observed and simulated values. However, because local contribution dominated the photochemical formation in urban Hong Kong, the discrepancy should not be large (Wang et al., 2017). In this study, the IOA reached 0.94 at the roadside MK site, and it decreased to 0.85 at the suburban TC site, possibly due to more regional transport of O_3 and VOC precursors from inland China to TC (Wang et al., 2017). High IOA values at both sites indicated high reliability of the in-situ photochemistry simulation in the study area.

2.3 O_3-precursors relationship

In this study, the O_3-precursors relationship was evaluated using the relative incremental reactivity (RIR), estimated based on the change in O_3 formation induced by the change in precursors levels (*i.e.,* NO_x, CO and VOCs). The RIR values are calculated from Equation 2 (Wang et al., 2017; Zeng et al., 2018):

$$RIR(X) = \frac{[P_{O_3}(X) - P_{O_3}(X - \Delta X)]/P_{O_3}(X)}{\Delta S(X)/S(X)} \quad (2)$$

where X refers to one specific precursor, S(X) represents the mixing ratio of the specific precursor, P_{O_3} represents the O_3 production rate in the unit of ppbv/h, ΔX is a hypothetical change in the mixing ratio of precursors. In this study, we assumed 10 % change in each type of precursor.

2.4 Scenario analysis

The impact of NO_x variation on in-situ photochemistry in urban environments was

obtained from the difference between a base scenario and a hypothetical scenario. In the base scenario, hourly data of air pollutants, including trace gases and VOCs, and meteorological parameters from 2013 to 2019 (2556 days in total) were input into the model to simulate the O_3 photochemistry during this period. In the hypothetical scenario, the NO_x values in 2013 remained unchanged in the following years (2014 - 2019), while the data of other pollutants and meteorological parameters were annually updated in the model using real measurement data from 2013 to 2019 as the settings in the base scenario. Radical concentrations (*i.e.*, OH, HO_2 and RO_2) and pathway reaction rates in O_3 photochemistry from 7 am to 7 pm in each sampling day were output in both scenarios, and converted into monthly averages for further analysis. The difference between base scenario and hypothetical scenario represented the impact of NO_x variation during 2014-2019 in urban Hong Kong, and offered the quantitative long-term effect of NO_x variations on O_3 photochemistry.

3 Results and discussion

3.1 NO_x observations in Hong Kong

Figure 2 and Figure 3 display the monthly average NO and NO_2 mixing ratios at 14 monitoring stations in Hong Kong during the study period. 95% confidence intervals were calculated for averaged values. Overall, significantly higher NO (135.7 ± 0.60 ppbv, $p < 0.01$) and NO_2 (54.0 ± 0.2 ppbv, $p < 0.01$) averages during 2007-2019 were captured at the roadside sites (MK and C) than those at other 12 general ambient sites (44.0 ± 0.09 ppbv for NO, 27.9 ± 0.02 ppbv for NO_2). This was mainly attributed to the dense vehicular emissions on the roadside, especially diesel-fueled vehicles and

buses, which are well known to emit large amounts of NO_x and particulate matter into the atmosphere. In general, mixing ratios of NO and NO_2 declined from 2007 to 2019, but the changing rates were not uniform across Hong Kong, as shown in Table S3. The reduction rates of NO ranged from 11.9 ± 0.6 to 14.9 ± 0.8 ppbv/yr ($p < 0.01$) at the roadside sites, and from 1.6 ± 0.2 to 4.4 ± 1.6 ppbv/yr ($p < 0.01$) at urban/suburban sites. Further, NO level at the rural site decreased insignificantly (p = 0.64). As for NO_2, it declined with decreasing rates of 1.6 ± 0.3 - 3.3 ± 0.3 ppbv/yr at the roadside sites, faster than those at the other sites (decreasing rates: 0.4 ± 0.1−1.6 ± 0.7 ppbv/yr). The results indicated that the effectiveness of vehicle emission control measures was more obvious at the roadside sites.

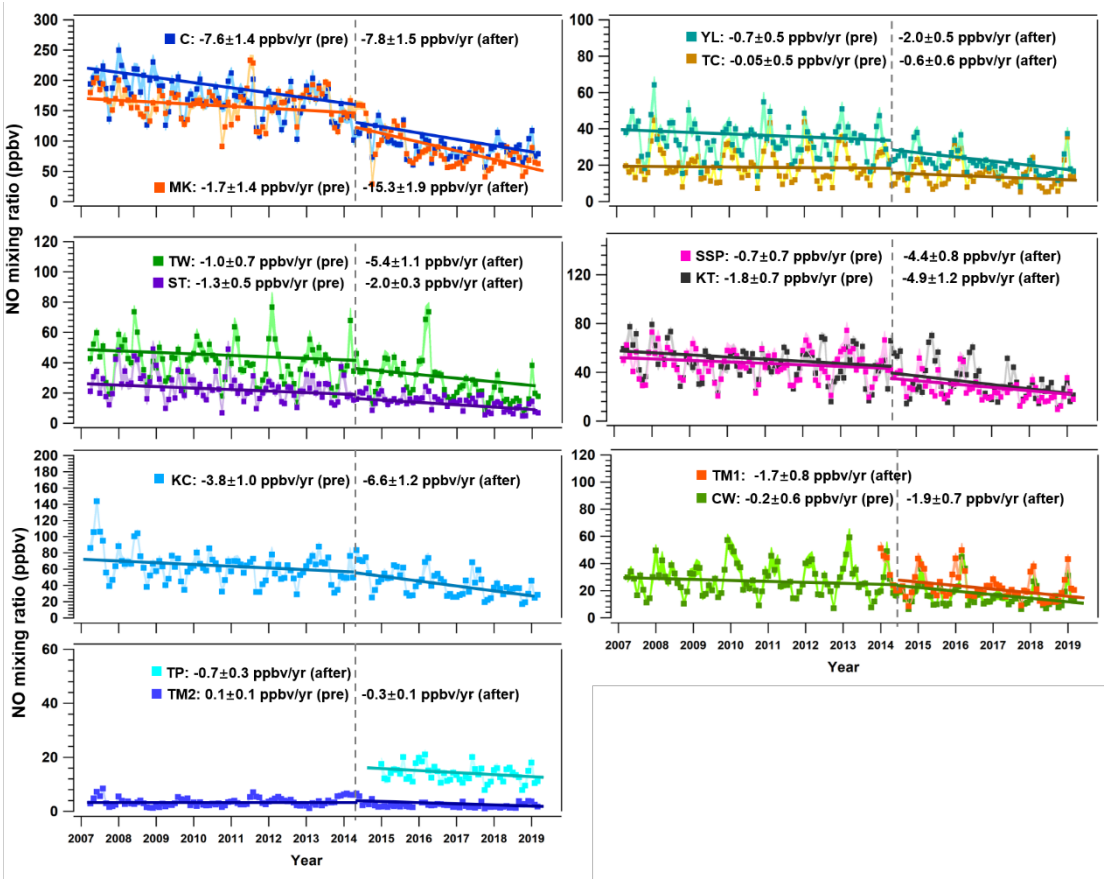

Figure 2. Monthly NO mixing ratios at 13 monitoring stations in Hong Kong during

Apr. 2007 – Mar. 2019. The grey dotted lines mark the start of the DCV Phase III program in Mar. 2014. The colored solid lines are the linear regressions of data points.

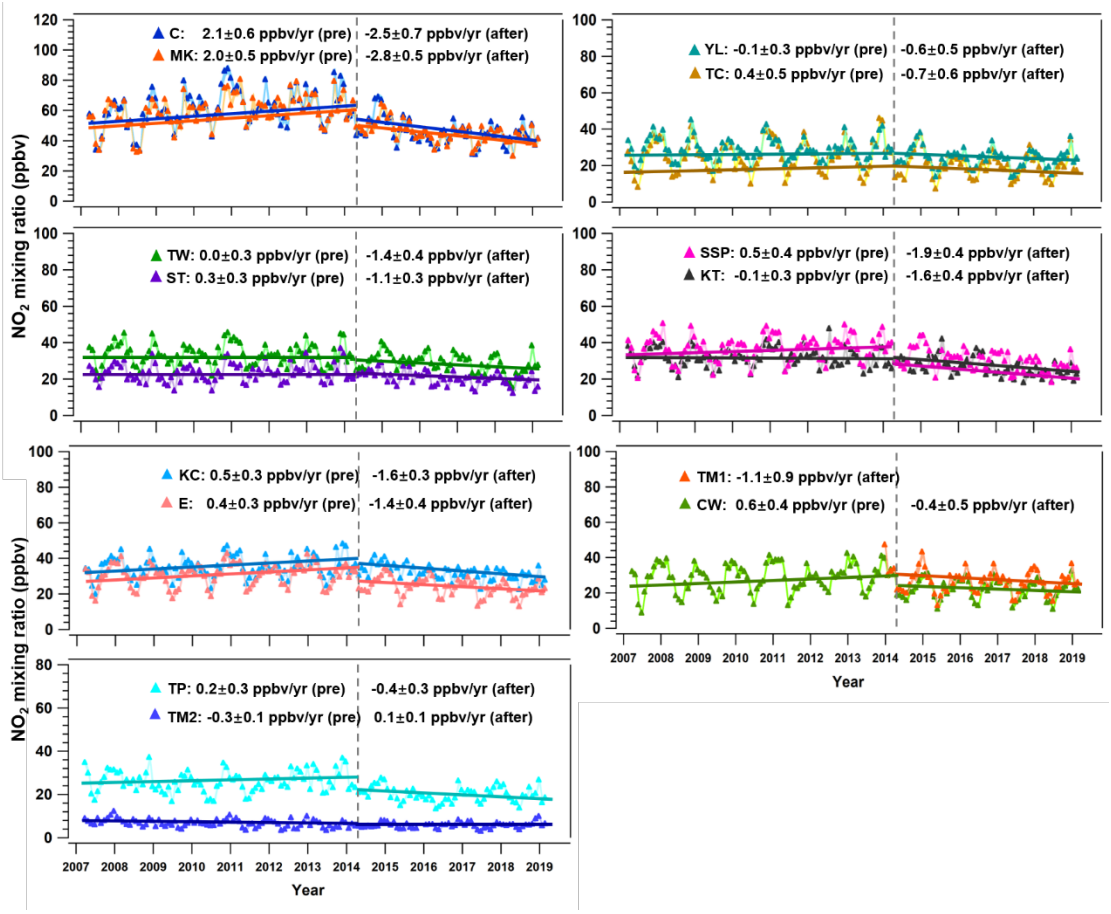

Figure 3. Monthly NO_2 mixing ratios at 14 monitoring stations in Hong Kong during Apr. 2007 – Mar. 2019. The grey dotted lines mark the start of the DCV Phase III in Mar. 2014. The colored solid lines are the linear regressions of data points.

To further look into the variation rates of NO_x in different periods, we selected March 2014 as the threshold since it was the starting point of DCV Phase III, dividing the whole study period into pre-DCV Phase III (including Phases I and II) and the DCV Phase III. Changing rates at each sampling site during the two phases are listed in Table S4. In general, NO reduced more rapidly after the implementation of DCV

196 Phase III, especially at the roadside MK site, where NO level declined at a rate of
197 15.3 ± 1.9 ppbv/yr, compared to 1.7± 1.4 ppbv/yr in pre-DCV Phase III. To minimize
198 the impact of meteorology in different years, the anomalies of NO and NO_2 were
199 calculated from 2007 to 2019 by taking the average value for each month and
200 subtracting the average for corresponding month over the whole study period (Text
201 S1). As shown in Figure S1, NO level at the roadside sites experienced a dramatic
202 drop-off due to the implementation of DCV Phase III, which kept obvious declining
203 afterward, indicated by the positive anomalies (32.3-33.3 ppbv) in pre-DCV Phase III
204 and negative anomalies (-51.7- -48.2 ppbv) during DCV Phase III. It is noteworthy
205 that though NO at the rural site remained unchanged in pre-DCV Phase III, it
206 significantly decreased (-0.3 ± 0.1 ppbv/yr) during the DCV Phase III. Different from
207 the NO trend, discernible rises in NO_2 level were identified at the roadside sites
208 before DCV Phase III with rates of 2.0 ± 0.5 - 2.1 ± 0.6 ppbv/yr ($p < 0.01$). However,
209 after the implementation of the DCV Phase III, NO_2 reduced at rates of 2.5 - 2.8 ppbv
210 per year ($p < 0.01$). Similar phenomena were found at other general ambient sites,
211 where NO_2 level remained stable before the DCV Phase III but began to decline after
212 that. Moreover, NO_2 anomalies in Figure S1 showed obvious differences before (5.5-
213 6.7 ppbv) and during (-8.7 - -8.2 ppbv) DCV Phase III.

214 Rising NO_2 level as well as NO_2/NO_x ratio were found in vehicle exhausts in previous
215 measurements (Carslaw et al., 2015; Smit et al., 2019). Here, we further investigated
216 the long-term variations of NO_2/NO_x ratio in the ambient air during 2007-2019, as
217 shown in Figure S2. Ratios recorded in this study (0.24-0.75) were found to be above

the range of the emission ratios (0.03-0.22) in the exhaust (Preble et al., 2015; Smit et al., 2019; Tian et al., 2011), which was reasonable due to the shorter atmospheric lifetime of NO compared to NO_2. Regarding temporal variations, NO_2/NO_x ratios were within 0.24-0.25 at roadside sites in 2017 and increased to 0.40-0.44 in 2019. The increased NO_2/NO_x ratio was possibly caused by intentional conversion of NO to NO_2 during the regeneration of diesel particulate filter (DPFs) (Preble et al., 2015; Smit et al., 2019). Higher NO_2/NO_x ratio at general sites than at roadside sites, increasing from 0.44-0.65 to 0.67-0.75, was mainly attributed to more secondary NO_2 formation in aged air masses.

To better elucidate the effectiveness of the DCV programs, source apportionment of 15 VOCs, CO, NO, NO_2 and SO_2 during 2014-2019 was conducted at the TC and MK sites (Figures S3 and S4). Model setting and the explanation of resolved factors were described in detail in Text S2. During the DCV Phase III, DCV emission on average accounted for $69.8 \pm 0.4\%$ and $63.0 \pm 0.4\%$ of ambient NO at MK and TC respectively, and $55.1 \pm 0.7\%$ and $32.8 \pm 0.3\%$ for ambient NO_2, respectively. Both NO and NO_2 at MK experienced pronounced decline of -14.4 ± 1.3 ppbv/yr ($p < 0.01$) and -5.1 ± 0.5 ppbv/yr ($p < 0.01$), respectively, during DCV Phase III. Similarly, NO and NO_2 had dramatic drop-off with reduction rates of 1.6 ± 0.3 ppbv/yr ($p < 0.01$) and 3.1 ± 0.5 ppbv/yr ($p < 0.01$) at TC site, respectively. Therefore, NO_x decreased in DCV exhaust were one of the main reasons of reductions in ambient NO_x. This result was in accordance with NO_x variation in the emission inventory, according to which NO_x emission kept decreasing during 2000-2018 and had larger reduction rate after

2014 (HKEPD, 2021). Since SCRs for NO_x removal were adopted in DCV Phase III (Table S1), it was reasonable that NO_x level decreased dramatically at this stage. The results confirmed the effectiveness of regulations implemented in DCV Phase III, including tightening emission standard and application of SCRs and DPFs, on controlling real-world NO_x level.

3.2 O_3 and VOCs observations in Hong Kong

Figure 4 shows the monthly O_3 variations at 14 monitoring stations in Hong Kong, respectively, during the study period. Generally, lower O_3 mixing ratio ($p < 0.01$) was observed at the roadside sites (9.8 ± 0.1 ppbv), due to more intensive NO titration, compared to that at general ambient sites (21.6 ± 0.02 ppbv). Ambient O_3 increased throughout the whole period with significance ($p < 0.05$) at most sites, with rates of 0.5 ± 0.2–3.2 ± 0.3 ppbv/yr (Table S3). Furthermore, no significant trends were identifiable before the implementation of DCV Phase III as shown in Table S4, while obvious O_3 increases ($0.3 \pm 0.5 – 2.4 \pm 0.6$ ppbv/yr, $p < 0.05$) were observed afterward at ten of the 14 sites. Besides, the number of O_3 episode days, defined as a day with maximum hourly O_3 value exceeding 80 ppbv, significantly ($p < 0.05$) increased at six sampling sites during 2007-2019, and peaked in 2019 at all sampling sites (Table S5).

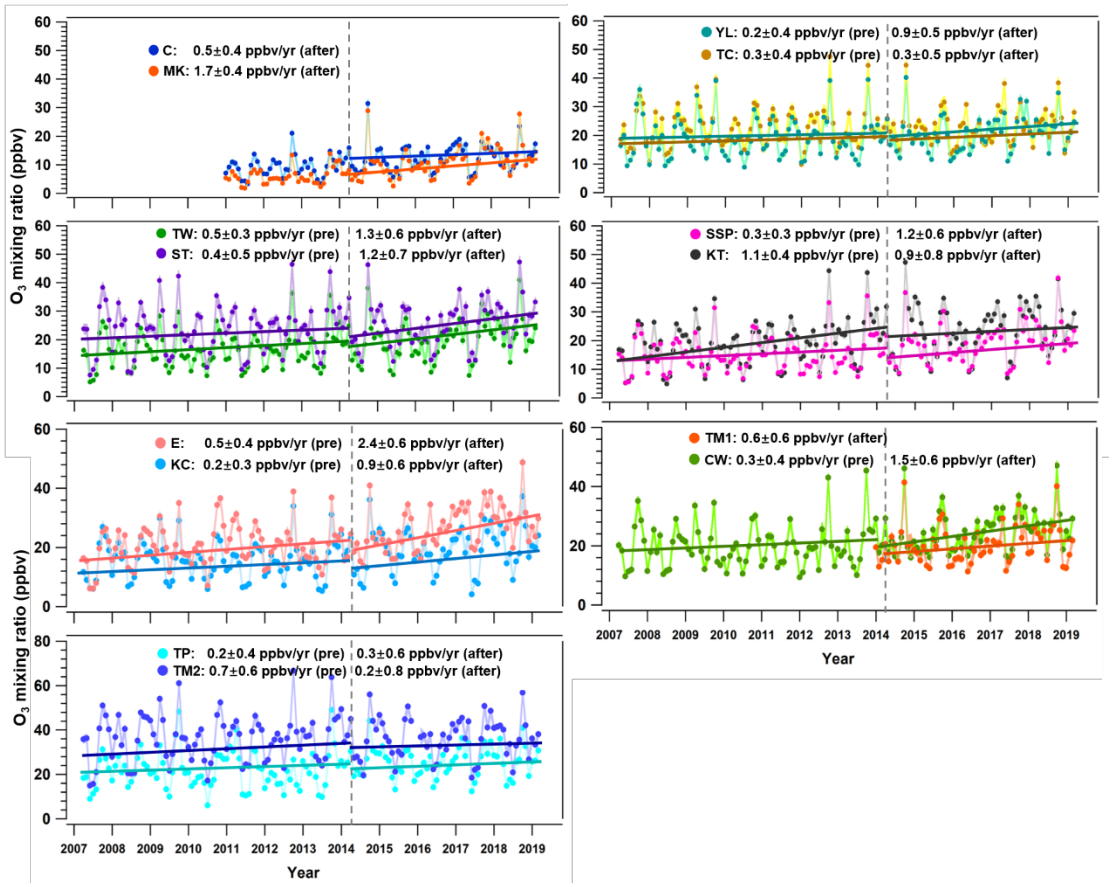

Figure 4. Monthly O_3 variations at 14 monitoring stations in Hong Kong during 2007-2019. Grey dotted lines indicate the start of DCV Phase III program in Mar. 2014. Colored solid lines are the linear regressions of data points.

As the O_3 precursors, the decline in NO_x levels might be an important chemical driving factor for O_3 increase in a VOC control regime. In addition, the significant increase in total VOCs (TVOCs) level (1.3 ± 0.5 ppbv/yr, $p < 0.05$, Figure S5) at the general ambient TC site during 2014-2019 would be another possible reason. Moreover, the OH reactivity of VOCs also increased dramatically at a rate of 0.4 ± 0.06 s^{-1}/yr ($p < 0.01$, Figure S5). However, TVOCs level reduced at a rate of 2.8 ± 0.5 ppbv/yr ($p < 0.01$, Figure S6) at the roadside MK site, so did the OH reactivity of VOCs (-0.2 ± 0.06 s^{-1}/yr, $p < 0.01$, Figure S6). It was noteworthy that VOCs derived

from DCV emission decreased at both TC and MK sites at rates of -0.4±0.07 and -1.7±0.2 ppbv/yr ($p < 0.01$), respectively, indicating the effectiveness of DCV Phase III in VOCs control. The difference in VOCs trends between roadside and suburban environments was probably due to different variations in local emission sources during 2014-2019, when biogenic emission increased significantly at TC (0.2±0.05, $p < 0.01$) but was invariable at MK. In addition to chemical driving factors, the impact of meteorology led to O_3 increase in suburban Hong Kong before 2012, while an obvious decreasing trend was observed after 2012 (Zeren et al., 2021, under review). The impact of meteorology on the long-term O_3 trend was insignificant ($p = 0.93$). Bearing the effectiveness of DCV Phase III in mind, especially for NO_x, it is of high necessity to investigate the impact of NO_x chemistry on O_3 trend in Hong Kong.

3.3 Variation trends of O_3-precursors relationships in different environments

The O_3-precursors relationship is essential for the planning and formulation of emission reduction policies to control O_3 pollution. Hence, O_3 formation sensitivity to different groups of precursors, including anthropogenic VOCs (AVOCs), biogenic VOCs (BVOCs), NO_x and CO, in urban environments in Hong Kong from 2013 to 2019 were investigated using the PBM-MCM model. The results are shown in Figure 5. In general, RIR values of AVOCs, BVOCs and CO were positive, while negative for NO_x at both sites, which meant that O_3 production was limited by VOCs and reduction in NO_x level led to O_3 increase in these years. At the roadside MK site, the average absolute RIR value of NO_x (1.6±0.03) was the highest, followed by AVOCs (1.2±0.04) and BVOCs (0.08±0.02), indicating the abundance of NO_x (86.3±2.1 ppbv)

and its dominant impact on O_3 formation in such NO_x-rich environment. Differently, the absolute RIRs of AVOCs (0.9±0.05) ranked first at the suburban TC site, followed by NO_x (0.7±0.05) and BVOCs (0.2±0.03), likely due to relatively low NO_x level (33.1±1.0 ppbv). The impact of CO on regulating O_3 formation was minor as its RIR values (0.02±0.01-0.03±0.004) at both sites were small. The findings agree with previous studies in Hong Kong (Guo et al., 2013; Wang et al., 2017). Here average RIR values before and after Mar. 2014 were calculated representing pre-DCV Phase III and DCV Phase III for intercomparison. The absolute RIR values of NO_x and AVOCs in pre-DCV Phase III were 1.7±0.06 and 1.3±0.09, larger than those (1.5±0.03 and 1.1±0.04) in DCV Phase III. At TC site, the absolute RIR of NO_x (0.9±0.09) during pre-DCV Phase III was also larger than that (0.7±0.05) in DCV Phase III. This result possibly indicated the decrease in sensitivity of NO_x at both sites and in AVOCs at MK to O_3 production.

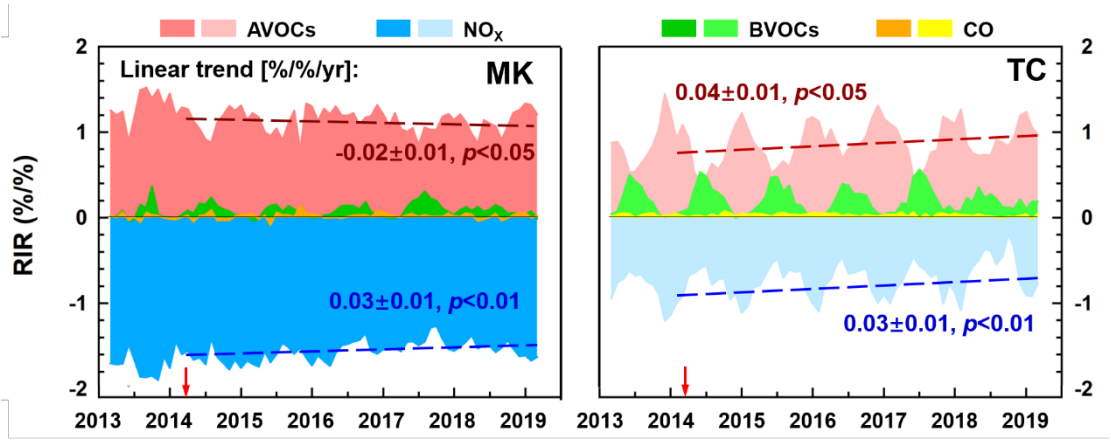

Figure 5. RIR values of O_3 precursors from 2013 to 2019 at MK site (left column) and TC site (right column). The linear trends during DCV Phase III are marked in colored lines and changing rates are shown inside the figures. Red arrows indicate the implementation of DCV Phase III.

The temporal variations of the RIRs were calculated after the implementation of DCV Phase III. RIRs of NO_x experienced an increase (p<0.01) at both sites with a growth rate of 0.03±0.01. Besides, the RIR values of AVOCs decreased dramatically (p<0.05) at MK site at a rate of -0.02±0.01, while increased (p<0.05) at TC site at a rate of 0.04±0.01 throughout the study period. Moreover, the sensitivities of BVOCs and CO to O_3 production remained unchanged (p>0.05) in these years. Overall, the evolution of RIRs implicated that O_3 production was less sensitive to its precursors (*i.e.,* NO_x and AVOCs) at the roadside MK station, implying that reduction in same percentage of precursors might lead to less O_3 decline in recent years. Consistently, O_3 formation became more sensitive to AVOCs at the suburban TC site, while it turned to be less sensitive to NO_x during the study period. More rapid decrease in NO_x than in VOCs by current findings might result in enhanced O_3 production. Hence, the next section will illustrate more detailed in-situ photochemistry in different environments.

3.4 Impact of NO_x reduction on in-situ O_3 photochemistry

In-situ O_3 photochemistry was simulated using the PBM-MCM model and the O_3 production and destruction rates were obtained during 7am-7pm for 2014-2019. Overall, the HO_2+NO pathway contributed more, with average percentages of 55% at MK and 58% at TC, than the RO_2+NO pathway to O_3 production in Hong Kong, but their reaction rates were both on a similar level. The reaction between RO_2 and NO contributed the remaining part (45% and 42%, respectively). In contrast, OH+NO_2 was the dominant destruction pathway of O_3 at both sites (98% at MK and 92% at TC). The results are consistent with those reported in other urban environments (Liu

et al., 2021; Lyu et al., 2019).

Figure 6 shows the monthly averaged changes in reaction rates of pathways in response to decreases of NO_x at MK and TC sites during 2014-2019 compared to 2013 in Hong Kong. Diurnal variations of changes in reaction rates were averaged during the whole period and shown in Figure 6 as well. Table S6 presents the percentage changes in reaction rates of pathways regulating O_3 production and oxidative radicals induced by NO_x reduction during 2014-2019 and converted into an average value representing the situation in the study period. At MK site, two O_3 formation pathways, *i.e.*, HO_2+NO and RO_2+NO, and the destruction pathway ($OH+NO_2$) were all facilitated by NO_x reduction, leading to an enhancement in net O_3 production rate during the whole period. Daytime net O_3 production rate increased by 0.7 ppbv/h (177%) in average during 2014-2019, when reaction rates of individual pathways increased by 0.43 ppbv/h (155%) for "HO_2+NO", 0.37 ppbv/h (160%) for "RO_2+NO" and 0.10 ppbv/h (99%) for "$OH+NO_2$". Variation rates of changes were calculated based on linear regression method. Changes in net O_3 production rate at MK increased significantly at a rate of 0.12±0.04 ppbv/h/yr (p<0.01), along with the continuous NO_x reduction. Besides, enhancements in "HO_2+NO", "RO_2+NO" and "$OH+NO_2$" increased at rates of 0.08±0.02, 0.07±0.02 and 0.02±0.004 ppbv/h/yr (p<0.01), respectively, as NO_x levels kept decreasing at the site. Similar situation was found at TC, where daily net O_3 production rate averagely enhanced by 4.0 ppbv/h (92%) and the enhancement increased at a rate of 0.24±0.05 ppbv/h/yr (p<0.01) during 2014-2019. Changes in reaction rates of production pathways "HO_2+NO" and

354 "RO_2+NO" were 0.7 ppbv/h (18%) and 0.3 ppbv/h (15%), increasing at rates of
355 0.13±0.03 and 0.10±0.02 ppbv/h/yr (p<0.01), respectively, while the change in
356 destruction pathway "OH+NO_2" was insignificant. Compared to TC site, larger
357 enhancement in net O_3 production rate at MK site was caused by higher NO_x
358 reduction at MK (108.5 ppbv, 42%) than at TC (11.9 ppbv, 25%). Overall, decreases
359 in NO_x resulted in more sufficient O_3 formation in urban environments in Hong Kong.

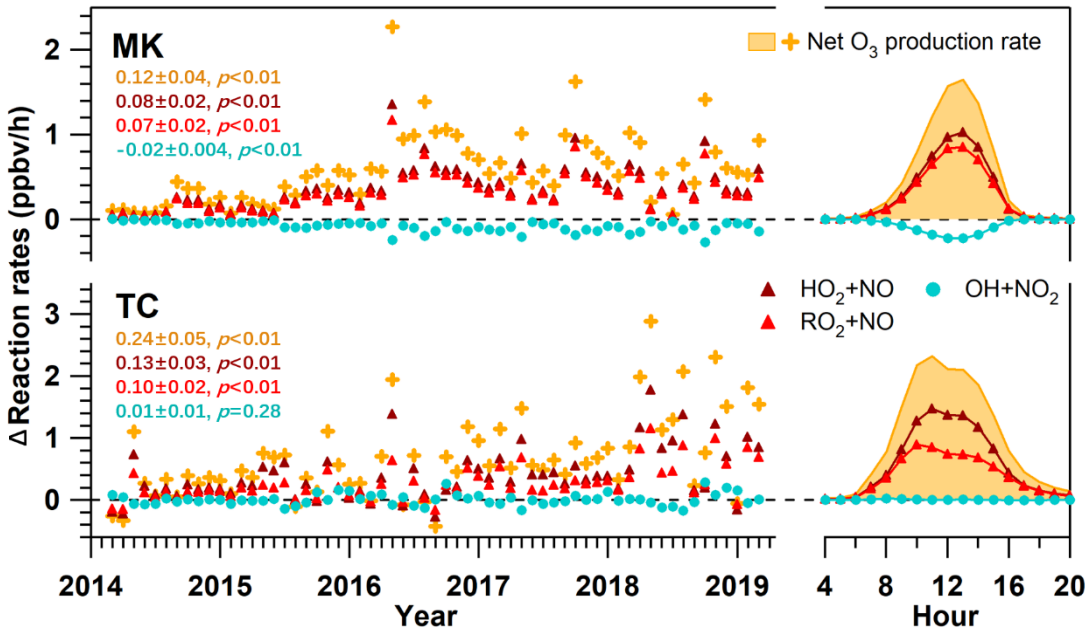

360

361 Figure 6. Monthly average changes (left) and diurnal variations of changes (right) in
362 reaction rates of pathways in response to deceases of NO_x at MK and TC sites during
363 2014-2019. Triangle and circular marks represent changes in production pathways and
364 destruction pathways, respectively. Cross marks and shaded area in orange stand for
365 the change in net O_3 production rate. Variation rates of changes in reaction rates were
366 listed in the same color as the marks (unit: ppbv/h/yr). Pathways with contributions
367 less than 5% are not shown.

368 To further investigate variations of atmospheric oxidative capacity caused by NO_x

reduction, the concentrations of RO_x radicals, including OH, HO_2 and RO_2 in 2014-2019 were simulated. Figure S7 shows the monthly average changes and diurnal variations of changes in RO_x radicals during 2014-2019 in response to NO_x reduction at MK and TC sites. Concentrations of OH, HO_2 and RO_2 radicals increased by 6.1×10^5 (402%), 9.2×10^5 (105%) and 1.4×10^6 molecules/cm^3/s (53%), respectively, in response to NO_x reduction at MK site. Besides, RO_x radicals enhanced more in concentrations but less in percentages at TC than at MK, by 7.8×10^5 (23%), 7.7×10^6 (35%) and 6.3×10^6 molecules/cm^3/s (32%) for OH, HO_2 and RO_2, respectively, induced by NO_x reduction. With regard to temporal variations, the enhancement in OH, HO_2 and RO_2 concentrations increased (p<0.05) at rates of $1.0\pm0.2\times10^5$, $0.7\pm0.3\times10^5$ and $0.6\pm0.2\times10^5$ molecules/cm^3/yr during 2014-2019 at MK, respectively, and at rates of $2.8\pm1.4\times10^5$, $4.9\pm1.3\times10^6$ and $3.7\pm0.8\times10^6$ molecules/cm^3/yr (p<0.05) at TC, respectively. We further looked into reaction rates in radical cycling for both OH and HO_2 and found that most of pathways were enhanced during 2014-2019 in response to NO_x reduction at both sites, as shown in Figures S8 and S9. Moreover, those enhancements kept increasing significantly (p<0.05) from 2014 to 2019 as NO_x levels decreased in Hong Kong. An exception was that the photolysis of HONO as well as its production through the reaction between OH and NO which participated in OH radical cycling were suppressed by NO_x reduction at TC, but enhanced at MK. This could be explained by the different variations in OH concentrations and NO levels at two sites. At MK, 42% reduction in NO_x level caused 192% increase in OH concentration, contributing to ~0.4ppbv/h

391 enhancement in pathways "HONO + *hv*" and "OH + NO" during the study period.
392 Differently, 25% decrease in NO_x resulted in 27% increment in OH concentration at
393 TC, which led to ~0.08ppbv/h suppression of these two pathways. Previous studies
394 mentioned that vehicle exhaust contributed to ambient HONO, which played an
395 important role in O_3 photochemistry (Kurtenbach et al., 2001). Yun et al. (2017)
396 reported that 38% of HONO was contributed by vehicle exhaust at MK site, where
397 DCVs accounted for 26% of the vehicle fleet. Zhang et al. (2016) found that only 2%
398 of ambient HONO came from traffic emissions. However, very limited studies
399 quantified the portion induced by DCV emissions. Model simulation indicated that 10%
400 of ambient HONO reduction caused 1% and 4% decreases in O_3 production rate at TC
401 and MK, respectively. In this study, we assumed an unchanged HONO emitted from
402 DCVs in Hong Kong to solely investigate the impact of NO_x reduction on in-situ
403 photochemistry.

404 To further reveal the role of NO_x in regulating the atmospheric oxidative capacity, a
405 sensitivity test was conducted by cutting 10% of NO_x as model input. Average
406 changes in reaction rates modulating OH, HO_2 and RO_2 concentrations during the
407 study period are shown in Figures S10-12. Table 1 summarizes the changes in sources,
408 sinks and cycling of radicals. At TC site, the NO_x reduction accelerated OH, HO_2 and
409 RO_2 productions by 0.017, 0.006 and 0.159 ppbv/h, leading to an increment in radical
410 cycling. At MK site, the decrease in NO_x facilitated HO_2 and RO_2 productions by
411 0.017 and 0.015 ppbv/h, but restrained OH production by 0.012 ppbv/h. The increase
412 in HO_2 and RO_2 radicals overwhelmed that in OH radical, further strengthening

413 radical cycling and contributing to oxidative capacity.

414 Table 1. Changes in reaction rates of pathways modulating OH, HO_2 and RO_2
415 concentrations in response to 10% reduction of NO_x (Unit: ppbv/h).

Site	TC			MK		
Radical	**OH**	**HO_2**	**RO_2**	**OH**	**HO_2**	**RO_2**
Source	-0.001	0.009	0.160	-0.001	0.017	0.015
Sink	-0.018	0.002	0.001	0.011	0.0001	0.0001
Net	0.017	0.006	0.159	-0.012	0.017	0.015
Cycling	0.241	0.267	0.224	0.358	0.232	0.174

416 **3.5 O_3 control measures**

417 To develop science-based control measures, variations in O_3-precursors relationships
418 were clarified by plotting isopleths of net O_3 production rate as a function of OH
419 reactivities of VOCs (OH reactivity$_{VOCs}$) and NO_x (OH reactivity$_{NOx}$) based on an
420 empirical kinetic modeling approach (EKMA) (Liu et al., 2021; Lyu et al., 2019). In
421 this study, OH reactivity is defined as the product of O_3 precursors (*i.e.,* VOCs and
422 NO_x) concentrations and the reaction rate constants between O_3 precursors and OH.
423 During 2013-2018, yearly average OH reactivity$_{VOCs}$ were within 67%-149% of the
424 overall average. As for OH reactivity$_{NOx}$, the range was 73-154%. To include OH
425 reactivities in all sampling years at both sites, hypotheses were made to cover
426 percentages from 0 to 200% with an interval of 10% of the OH reactivity for both
427 VOCs and NO_x. Using the PBM-MCM model, we simulated 441 scenarios and
428 extracted maximum net O_3 production rates that occurred at 13:00 LT in each scenario
429 to obtain the isopleths, as shown in Figure 7.

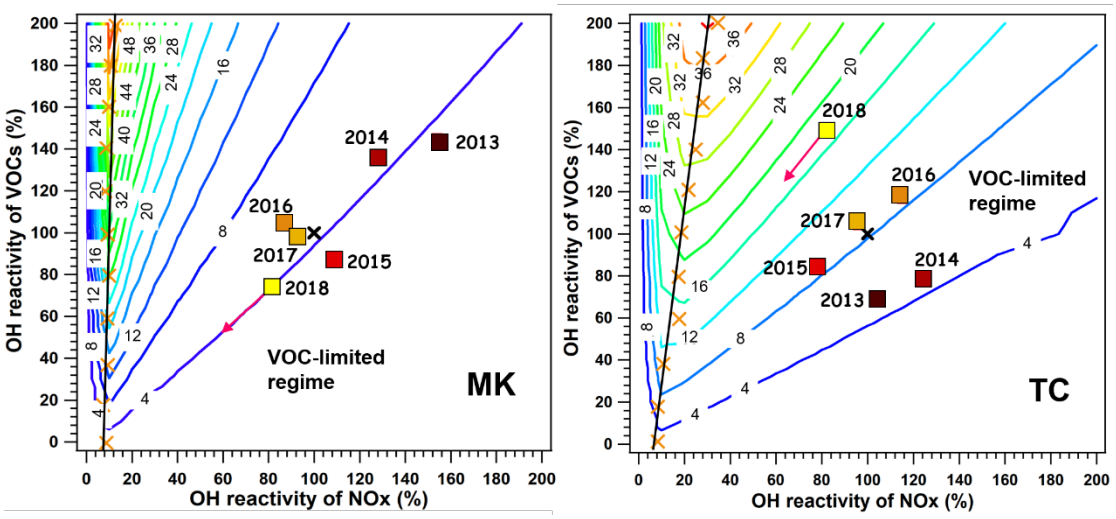

Figure 7. Average isopleth of net O_3 production rate (ppbv/hr) at 13:00 LT as a function of OH reactivity$_{VOCs}$ and OH reactivity$_{NOx}$ at MK (left) and TC (right) sites. The colored squares represent calculated yearly average OH reactivity$_{VOCs}$ and OH reactivity$_{NOx}$ at 13:00 LT from 2013 to 2018. Orange crosses denote the OH reactivity$_{VOCs}$ and OH reactivity$_{NOx}$ at 13:00 LT with the highest net O_3 production rate at each given OH reactivity$_{VOCs}$. Black cross represents the base case, referring to the overall average during the whole sampling period. Solid black line derives from the linear regression of orange crosses and divides O_3 formation into VOCs-limited regime and NO_x-limited regime. Pink arrow represents the tangent line of the isopleth for 2018 data.

O_3 formation regimes were defined at both TC and MK sites during the study period. Detailed description of this approach is given in Text S3. The isopleths indicated that O_3 formation was controlled by VOCs at both MK and TC sites from 2013 to 2018, which meant that cutting VOCs emission would be more effective to suppress O_3 production in Hong Kong. At MK site, the O_3 production rate was the lowest in 2013,

and increased during 2014-2015 due to the declined OH reactivity$_{VOCs}$ and OH reactivity$_{NOx}$. From 2016 to 2017, the combined effect of decreased OH reactivity$_{NOx}$ and increased OH reactivity$_{VOCs}$ led to an obvious rise in O_3 production. Although OH reactivity$_{VOCs}$ reached the lowest value during the study period in 2018, the net O_3 production rate still exceeded that in 2013 due to continuous decreasing OH reactivity$_{NOx}$. At TC site, O_3 production rate increased by ~12 ppbv/h from 2013 to 2018, owing to 21% reduction in OH reactivity$_{NOx}$ and 80% increment in OH reactivity$_{VOCs}$. In view of the remarkable drop in ambient NO_x in Hong Kong in the past decade, the O_3 control strategies in such a VOCs-limited regime have proposed stricter requirements for cutting VOCs emissions. Based on pollutant profiles in 2018, the ratio of OH reactivity reduction between VOCs and NO_x should be larger than 1 at MK site and 1.3 at TC site for O_3 abatement (indicated by pink arrows in Figure 7).

4 Implications

In this work, we found that after the implementation of DCV Phase III, the reduction rates of NO and NO_2 were both greater than before. Furthermore, NO_x reduction was more significant in roadside environment than in suburban/urban environments. Source apportionment results confirmed the decline in NO_x from diesel vehicle emissions in these years. Besides, increasing NO_2/NO_x ratio were recorded, possibly due to the wide application of DPFs. Generally, O_3 increased faster after the implementation of DCV Phase III, largely attributed to dramatic NO_x reduction. To verify the inference, the PBM-MCM model for the first time was applied to evaluate the impact of NO_x reduction on O_3 photochemistry in two microenvironments in

Hong Kong. During 2014-2019, the net O_3 production rate was more than doubled because of 42% of NO_x reduction in the roadside environment. Owing to NO_x reduction, OH, HO_2 and RO_2 radicals were 1.5 to 5 times those in pre-DCV Phase III period. In suburban environment, declines in NO_x also led to enhancement in atmospheric oxidative capacity, but the change in O_3 production rate was smaller than that at the roadside site. Isopleth of net O_3 production rate revealed that O_3 formation was controlled by VOCs in Hong Kong during the sampling period. To alleviate O_3 pollution, the result suggests the reduction ratio of OH reactivity between VOCs and NO_x should be larger than 1 at the roadside site and 1.3 in the suburban area, until the control regime switches to transitional or NO_x-limited regime. In other words, confining VOC emissions is a key step for Hong Kong to control O_3 at this stage, especially those VOCs with high OH reactivities. To sum up, this study reveals that NO_x reduction due to the implementation of DCV emission control measures led to continuous increase in O_3 in Hong Kong. The findings contributed to a more comprehensive understanding of the O_3 photochemistry associated with NO_x variations in various environments.

Acknowledgements

This study was supported by the Research Grants Council of the Hong Kong Special Administrative Region via Theme-Based Research Scheme (T24-504/17-N), the NSFC/RGC joint scheme (N_PolyU530/20), General Research Fund (PolyU15212421), the Strategic Focus Area scheme of The Research Institute for Sustainable Urban Development, Hong Kong Polytechnic University (1-BBW9), and

Guangdong Basic and Applied Basic Research Foundation (2021A1515110297).

References

Atkinson, R. Atmospheric chemistry of VOCs and NO_X. *Atmos. Environ.* **2000**, 34(12), 2063-2101.

Bell, M. L.; McDermott, A.; Zeger, S. L.; Samet, J. M. and Dominici, F. Ozone and Short-term Mortality in 95 US Urban Communities, 1987-2000. *JAMA*, **2004**, 292(19), 2372-2378.

Beevers, S. D.; Westmoreland, E.; de Jong, M. C.; Williams, M. L. and Carslaw, D. C. Trends in NOx and NO2 emissions from road traffic in Great Britain. *Atmos. Environ.* **2012**, 54, 107-116.

Carslaw, D. C.; Priestman, M.; Williams, M. L.; Stewart, G. B. and Beevers, S. D. Performance of optimised SCR retrofit buses under urban driving and controlled conditions. *Atmos. Environ.* **2015**, 105, 70–77.

Carslaw, D.; Beevers, S.; Westmoreland, E.; Williams, M.; Tate, J.; Murrells, T.; Stedman, J.; Li, Y.; Grice, S.; Kent, A. and Tsagatakis, I. Trends in NOx and NO2 emissions and ambient measurements in the UK. *Defra, London*. **2011**, version 18th July.

EEA. National emissions reported to the Convention on Long-range Transboundary Air Pollution (LRTAP Convention) provided by European Environmental Agency, **2015**. Available from: https://www.eea.europa.eu/data-and-maps/daviz/sector-share-of-nitrogen-oxides-emissions#tab-chart_1.

511 Geddes, J. A.; Murphy, J. G. and Wang, D. K. Long term changes in nitrogen oxides
512 and volatile organic compounds in Toronto and the challenges facing local ozone
513 control. *Atmos. Environ.* **2009**, 43, 3407-3415.

514 Guan, B.; Zhan, R.; Lin, H. and Huang, Z. Review of state of the art technologies of
515 selective catalytic reduction of NOx from diesel engine exhaust. *Appl. Therm. Eng.*
516 **2014**, 66(1-2), 395-414.

517 Guo, H., Ling, Z. H., Cheung, K., Jiang, F., Wang, D. W., Simpson, I. J., Barletta, B.,
518 Meinardi, S., Wang, T. J., Wang, X. M., Saunders, S. M., and Blake, D. R.:
519 Characterization of photochemical pollution at different elevations in mountainous
520 areas in Hong Kong. *Atmos. Chem. Phys.* **2013**, 13, 3881-3898.

521 HKEPD. Hong Kong Air Pollutant Emission Inventory, **2021**. Available from:
522 https://www.epd.gov.hk/epd/english/environmentinhk/air/data/emission_inve.html.

523 HKEPD. Hong Kong Air Pollutant Emission Inventory - Nitrogen Oxides, **2020**.
524 Available from:
525 https://www.epd.gov.hk/epd/english/environmentinhk/air/data/emission_inve_nox_P.h
526 tml.

527 HKEPD. Cleaning the Air at Street Level, **2019a**. Available from:
528 https://www.epd.gov.hk/epd/english/environmentinhk/air/prob_solutions/cleaning_air
529 _atroad.html.

530 HKEPD. Air quality in Hong Kong 2019, **2019b**. Available from:
531 https://www.aqhi.gov.hk/api_history/english/report/files/AQR2019e_final.pdf.

Hoek, G.; Brunekreef, B.; Goldbohm, S.; Fischer, P. and van den Brandt, P. A. Association between mortality and indicators of traffic-related air pollution in the Netherlands: a cohort study. *The Lancet.* **2002**, 360 (9341), 1203–1209.

Itano, Y.; Bandow, H.; Takenaka, N.; Saitoh, Y.; Asayama, A. and Fukuyama, J. Impact of NOx reduction on long-term ozone trends in an urban atmosphere. *Sci. Total Environ.* **2007**, 379, 46-55.

Jiang, J. B. and Li, D. G. Theoretical analysis and experimental confirmation of exhaust temperature control for diesel vehicle NO_x emissions reduction. *Appl. Energy.* **2016**, 174, 232-244.

Kurtenbach, R.; Becker, K. H.; Gomes, J. A. G.; Kleffmann, J.; Lörzer, J. C.; Spittler, M.; Wiesen, P.; Ackermann, R.; Geyer, A. and Platt, U. Investigations of emissions and heterogeneous formation of HONO in a road traffic tunnel. *Atmos. Environ.* **2001**, 35(20), 3385-3394.

Li, K.; Jacob, D. J.; Shen, L.; Lu, X.; Smedt, I. D. and Liao, H. Increases in surface ozone pollution in China from 2013 to 2019: anthropogenic and meteorological influences. *Atmos. Chem. Phys.* **2020**, 20, 11423-11433.

Liu, Y. M. and Wang, T. Worsening urban ozone pollution in China from 2013 to 2017 - Part 2: The effects of emission changes and implications for multi-pollutant control. *Atmos. Chem. Phys.* **2020**, 20, 6323-6337.

Liu, X. F.; Guo, H.; Zeng, L. W.; Lyu, X. P.; Wang, Y.; Zeren, Y. Z.; Yang, J.; Zhang, L. Y.; Zhao, S. Z.; Li, J. and Zhang, G. Photochemical ozone pollution in five Chinese

553 megacities in summer 2018. *Sci. Total Environ.* **2021**, 801, 149603.

554 Liu, X. J.; Xu, W.; Du, E. Z.; Tang, A. H.; Zhang, Y.; Zhang, Y. Y.; Wen, Z.; Hao, T.
555 X.; Pan, Y. P.; Zhang, L.; Gu, B. J.; Zhao, Y.; Shen, J. L.; Zhou, F.; Gao, Z. L.; Feng, Z.
556 Z.; Chang, Y. H.; Goulding, K.; Collett Jr, J. L.; Vitousek, P. M. and Zhang, F. S.
557 Environmental impacts of nitrogen emissions in China and the role of policies in
558 emission reduction. *Phil. Trans. R. Soc. A*, **2020**, 378.

559 Lu, H. X.; Lyu, X. P.; Cheng, H. R.; Ling, Z. H. and Guo, H. Overview on the spatial-
560 temporal characteristics of the ozone formation regime in China. *Environ. Sci.:*
561 *Process. Impacts*. **2019**, 21 (6), 916-929.

562 Lu, X.; Zhang L.; Wang, X. L.; Gao, M.; Li, K.; Zhang, Y. Z.; Yue, X. and Zhang, Y.
563 H. Rapid Increases in Warm-Season Surface Ozone and Resulting Health Impact in
564 China Since 2013. *Environ. Sci. Technol. Lett.* **2020**, 7, 240-247.

565 Lyu, X. P.; Wang, N.; Guo, H.; Xue, L. K.; Jiang, F.; Zeren, Y. Z.; Cheng, H. R.; Cai,
566 Z.; Han, L. H. and Zhou, Y. Causes of a continuous summertime O3 pollution event in
567 Jinan, a central city in the North China Plain. *Atmos. Chem. Phys.* **2019**, 19, 3025-
568 3042.

569 Lyu, X. P.; Zeng, L. W.; Guo, H.; Simpson, I. J.; Ling, Z. H.; Wang, Y.; Murray, F.;
570 Louie, P. K. K.; Saunders, S. M.; Lam, S. H. M. and Blake, D. R. Evaluation of the
571 effectiveness of air pollution control measures in Hong Kong. *Environ. Pollut.* **2017**,
572 220, 87-94.

573 Lyu, X. P.; Guo, H.; Simpson, I. J.; Meinardi, S.; Louie, P. P. K.; Ling, Z. H.; Wang, Y.;

574 Liu, M.; Luk, W. Y.; Wang, N. and Blake, D. R. Effectiveness of replacing catalytic
575 converters in LPG-fueled vehicles in Hong Kong. *Atmos. Chem. Phys.* **2016**, 16,
576 6609-6626.

577 Macdonald, E., Otero, N., and Butler, T. A comparison of long-term trends in
578 observations and emission inventories of NOx. *Atmos. Chem. Phys.* **2021**, 21, 4007–
579 4023.

580 Pandey, S. K.; Kim, K. H.; Chung, S. Y; Cho, S. J.; Kim, M. Y. and Shon, Z. H. Long-
581 term study of NOx behavior at urban roadside and background locations in Seoul,
582 Korea. *Atmos. Environ.* **2008**, 42, 607-622.

583 Preble, C. V.; Dallmann, T. R.; Kreisberg, N. M.; Hering, S. V.; Harley, R. A. and
584 Kirchstetter, T. W. Effects of particle filters and selective catalytic reduction on heavy-
585 duty diesel drayage truck emissions at the Port of Oakland. *Environ. Sci. Technol.*
586 **2015**, 49(14), 8864-8871.

587 Reşitoğlu, I. A.; Altinişik, K. and Keskin, A. The pollutant emissions from diesel-
588 engine vehicles and exhaust aftertreatment systems. *Clean Technol. Environ. Policy.*
589 **2015**, 17, 15-27.

590 Samoli, E.; Aga, E., Touloumi, G.; Nisiotis, K.; Forsberg, B.; Lefranc, A.; Pekkanen,
591 J.; Wojtyniak, B.; Schindler, C.; Niciu, E.; Brunstein, R.; Dodic Fikfak, M.; Schwartz,
592 J. and Katsouyanni, K. Short-term effects of nitrogen dioxide on mortality: An
593 analysis within the APHEA project. *Eur. Respir. J.* **2006**, 27(6), 1129–1138.

594 Shon, Z. H.; Kim, K. H.; Song, S. K. Long-term trend in NO2 and NOx levels and

595 their emission ratio in relation to road traffic activities in East Asia. *Atmos. Environ.*
596 **2011**, 45, 3120-3131.

597 Simon, H.; Reff, A.; Wells, B.; Xing, J. and Frank, N. Ozone Trends Across the
598 United States over a Period of Decreasing NOx and VOC Emissions. *Environ. Sci.*
599 *Technol.* **2015**, 49(1), 186–195.

600 Smit, R.; Keramydas, C.; Ntziachristos, L.; Lo, T. S.; Ng, K. L.; Wong, H. L. and
601 Wang, C. K. L. Evaluation of Real-World Gaseous Emissions Performance of
602 Selective Catalytic Reduction and Diesel Particulate Filter Bus Retrofits. *Environ. Sci.*
603 *Technol.* **2019**, 53, 4440-4449.

604 Takekawa, H.; Chatani, S. and Ito, A. A new approach for estimation of the effect of
605 NOx emission reduction on roadside NO_2 concentration in Tokyo. *Atmos. Environ.*
606 **2013**, 68, 92-102.

607 Teshirogi, N. and H. Nakahara. Method For Controlling Noxious Components Of
608 Exhaust Gas From Diesel Engine. *US Patent*, **1974**, US3851632A.

609 Tian, L. W.; Hossain, S. R.; Lin, H. L.; Ho, K. F., Lee, S. C. and Yu, I. T. S. Increasing
610 trend of primary NO_2 exhaust emission fraction in Hong Kong. *Environ. Geochem.*
611 *Hlth.* **2011**, 33, 623-630.

612 Vohra, K.; Marais, E. A.; Suckra, S., Kramer, L.; Bloss, W. J.; Sahu, R.; Gaur, A.;
613 Tripathi, S. N.; Van Damme, M.; Clarisse, L. and Coheur, P.-F. Long-term trends in air
614 quality in major cities in the UK and India: a view from space. *Atmos. Chem. Phys.*
615 **2021**, 21, 6275–6296.

Wang, N.; Lyu, X. P.; Deng, X. J.; Huang, X.; Jiang, F. and Ding, A. J. Aggravating O3 pollution due to NOx emission control in eastern China. *Sci. Total Environ.* **2019**, 677, 732–744.

Wang, Y.; Wang, H.; Guo, H.; Lyu, X. P.; Cheng, H. R.; Ling, Z. H.; Louie, P. K. K.; Simpson, I. J.; Meinardi, S. and Blake, D. R. Long term O3-precursor relationships in Hong Kong: Field observation and model simulation. *Atmos. Chem. Phys.* **2017**, 17, 10919-10935.

Wu, Y.; Zhang, S. J.; Li, M. L.; Ge, Y. S.; Shu, J. W.; Zhou, Y.; Xu, Y. Y.; Hu, J. N.; Liu, H.; Fu, L. X.; He, K. B. and Hao, J. M. The challenge to NOx emission control for heavy-duty diesel vehicles in China. *Atmos. Chem. Phys.* **2012**, 12, 9365-9379.

Yun, H.; Wang, Z.; Zha, Q. Z.; Wang, W. H.; Xue, L. K.; Zhang, L.; Li, Q. Y.; Cui, L.; Lee, S. C.; Poon, S. C. N. and Wang, T. Nitrous acid in a street canyon environment: Sources and contributions to local oxidation capacity. *Atmos. Environ.* **2017**, 167, 223-234.

Zeng, L. W.; Lyu, X.P.; Guo, H.; Zou, S. C. and Ling, Z. H. Photochemical formation of C_1-C_5 alkyl nitrates in suburban Hong Kong and over South China Sea. *Environ. Sci. Technol.* **2018**, 52, 5581-5589.

Zeren, Y. Z.; Guo, H.; Lyu, X. P.; Zhou, B. N.; Liu, X. F.; Yang, L. F.; Yuan, Z. B. and Wang, Y. Remarkable spring increase overwhelmed hard-earned autumn decrease in ozone pollution from 2005 to 2017 in Hong Kong, South China. Available at SSRN: https://dx.doi.org/10.2139/ssrn.3994604.

637 Zhang, L.; Wang, T.; Zhang, Q.; Zheng, J. Y.; Xu, Z. and Lv, M. Y. Potential sources
638 of nitrous acid (HONO) and their impacts on ozone: A WRF-Chem study in a polluted
639 subtropical region. *J. Geophys. Res. Atmos.* **2016**, 121, 7, 3645-3662.

640 Zhang, Q.; Zheng, Y. X.; Tong, D.; Shao, M.; Wang, S. X.; Zhang, Y. H.; Xu, X. D.;
641 Wang, J. N.; He, H.; Liu, W. Q.; Ding, Y. H.; Lei, Y.; Li, J. H.; Wang, Z. F.; Zhang, X.
642 Y.; Wang, Y. S.; Cheng, J.; Liu, Y.; Shi, Q. R.; Liu, Y.; Geng, G. N.; Hong, C. P.; Li,
643 M.; Liu, F.; Zheng, B.; Cao, J. J.; Ding, A. J.; Gao, J.; Fu, Q. Y.; Huo, J. T.; Liu, B. X.;
644 Liu, Z. R.; Yang, F. M.; He, K. B. and Hao, J. M. Drivers of improved PM2.5 air
645 quality in China from 2013 to 2017. *PNAS*. **2019**, 116 (49) 24463-24469.

646 Zhang, Q.; Yuan, B.; Shao, M.; Wang, X.; Lu, S.; Lu, K.; Wang, M.; Chen, L.; Chang,
647 C. C. and Liu, S. C. Variations of ground-level O3 and its precursors in Beijing in
648 summertime between 2005 and 2011. *Atmos. Chem. Phys.* **2014**, 14, 6089-6101.

649 Zhao, B.; Wang, S. X.; Wang, J. D.; Fu, J. S.; Liu, T. H.; Xu, J. Y.; Fu, X. and Hao, J.
650 M. Impact of national NOx and SO2 control policies on particulate matter pollution in
651 China. *Atmos. Environ.* **2013**, 77, 453-463.